Inductor-Free Wireless Energy Delivery via Maxwell's Displacement Current from an Electrodeless Triboelectric Nanogenerator

Xia Cao, Meng Zhang, Jinrong Huang, Tao Jiang, Jingdian Zou, Ning Wang, and Zhong Lin Wang**

Wireless power delivery has been a dream technology for applications in medical science, security, radio frequency identification (RFID), and the internet of things, and is usually based on induction coils and/or antenna. Here, a new approach is demonstrated for wireless power delivery by using the Maxwell's displacement current generated by an electrodeless triboelectric nanogenerator (TENG) that directly harvests ambient mechanical energy. A rotary electrodeless TENG is fabricated using the contact and sliding mode with a segmented structure. Due to the leakage of electric field between the segments during relative rotation, the generated Maxwell's displacement current in free space is collected by metal collectors. At a gap distance of 3 cm, the output wireless current density and voltage can reach 7 μA cm^{-2} and 65 V, respectively. A larger rotary electrodeless TENG and flexible wearable electrodeless TENG are demonstrated to power light-emitting diodes (LEDs) through wireless energy delivery. This innovative discovery opens a new avenue for noncontact, wireless energy transmission for applications in portable and wearable electronics.

Prof. X. Cao, M. Zhang, J. Huang, Prof. T. Jiang, J. Zou, Prof. Z. L. Wang
Beijing Institute of Nanoenergy and Nanosystems
Chinese Academy of Sciences
University of Chinese Academy of Sciences
Beijing 100083, China
E-mail: zlwang@gatech.edu

Prof. X. Cao
Research Center for Bioengineering and Sensing Technology
Beijing Key Laboratory for Bioengineering and Sensing Technology
School of Chemistry and Biological Engineering
University of Science and Technology Beijing
Beijing 100083, China

Prof. N. Wang
Center for Green Innovation
School of Mathematics and Physics
University of Science and Technology Beijing
Beijing 100083, China
E-mail: wangning@ustb.edu.cn

Prof. N. Wang, Prof. Z. L. Wang
School of Material Science and Engineering
Georgia Institute of Technology
Atlanta, GA 30332-0245, USA

Prof. Z. L. Wang
CAS Center for Excellence in Nanoscience
National Center for Nanoscience and Technology (NCNST)
Beijing 100190, China

The ORCID identification number(s) for the author(s) of this article can be found under https://doi.org/10.1002/adma.201704077.

DOI: 10.1002/adma.201704077

Energy is the foundation of today's society. Ever since the first utilization of electric power, electricity is always transmitted via metal wires/cables with high efficiency, high security, and precise delivery. Electromagnetic generator (EMG) has been the dominant technology for power generation in fossil fuel, nuclear, and hydrodynamic power plants. EMG relies on the Lorentz force driven flow of free electrons in a metal coil. Meanwhile, to meet the needs of today's mobile electronics, Internet of things, and sensor networks, wireless delivery of electric power is essential for some applications particularly for implantable medical devices and security. Compared to the importance of wireless communication technology, wireless charging technology is also highly desirable to enhance the adaptability and mobility of wireless devices and systems.[1–6] Although there are three modes of wireless charging technology including electromagnetic induction, magnetic resonance, and radio wave, all of them are rather inefficient and complex.[7]

Recently, triboelectric nanogenerators (TENG) have been invented and developed for harvesting small-scale ambient mechanical energy for building self-powered systems. TENG is particularly advantageous at low operation frequency (<5 Hz) in comparison with the traditional EMG, so that it is most effective for power generation utilizing the actions existing in nature and in our living environment.[8] A variety of TENGs and related self-powered systems have been reported based on four fundamental working modes that can scavenge mechanical energy from mechanical triggering, human motion, wind blowing, water flowing, and so on.[9–16] These features make TENG far different from another important member of the nanogenerator family, namely, piezoelectric nanogenerator.[17,18] Recently, the fundamental physics for energy harvesting by nanogenerators has been found to be derived from the second term of Maxwell's displacement current.[19,20] It is also presented that displacement current will hugely impact the technological developments of Internet of things, sensor network, blue energy, and big data in the clear future prediction.

Here, we demonstrate a newly designed electrodeless TENG for wireless energy delivery by utilizing the relative rotations between a polypropylene (PP) disk and polymethyl methacrylate

(PMMA) sectors. The metal collectors can harvest the energy wirelessly from the time-varying electric displacement field based on Maxwell's displacement current. For such an as-designed rotary electrodeless TENG, the output current density via collectors can reach 7 μA cm^{-2} and the open-circuit voltage reaches 65 V at the vertical distance of 3 cm. Especially, the distance of wireless energy delivery can be as long as 18 cm at the present stage, making it feasible for noncontact devices and collectors. This work introduces the electrodeless TENG based on Maxwell's displacement current that can wirelessly harvest ambient mechanical energy to sustainably power a broad range of portable and wearable electronic devices.

The electrodeless TENG can work and output periodic electric signals in the absence of metal electrodes and wires, which is distinctly different from the present single- or dual-electrode TENGs. Here the TENG is called as electrodeless TENG to emphasize its essential and distinctive difference from those TENGs reported in previous works. Usually, the electrodes are deposited onto the backsides of dielectric materials or serve directly as the triboelectric materials to contact/separate with dielectric materials. However, no metal electrodes are needed to be deposited on the main body in the TENG in our current work. The power produced by such a newly designed TENG can be conveniently collected by metal collectors and stored for general applications. The working mechanism of the electrodeless TENG can be demonstrated by the finite element simulations. We mainly focused on a rotary electrodeless TENG consisting of a PP disk and PMMA sectors. A 3D theoretical model for such TENG corresponding to the experiment was constructed and shown in **Figure 1**a. The 5 mm thick PP disk acts as the stator, and the 5 mm thick PMMA sectors with four units can rotate clockwise around the central axis of TENG (the rotating angle is represented by θ). The inner and outer diameters were fixed as 3 and 25 cm. The charge density on the lower face of the PMMA sector was assigned as $+2\sigma$, and that on the upper face of PP disk was $-\sigma$. Therefore, the net charge density

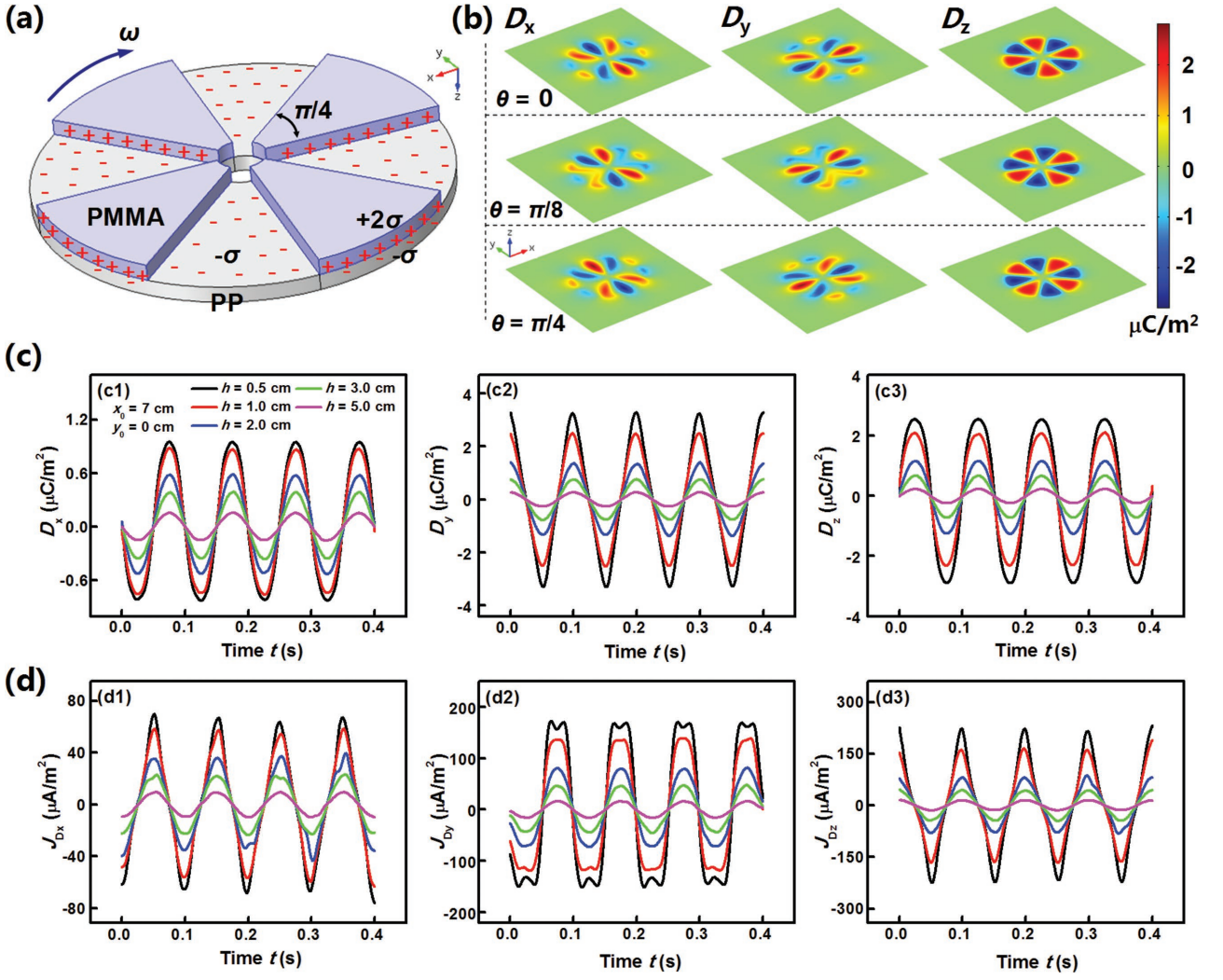

Figure 1. Working mechanism of the electrodeless TENG. a) Theoretical model built for the rotary electrodeless TENG with a PP disk and PMMA sectors. b) Field distributions of electric displacements in *x*-, *y*-, and *z*-directions at a constant height ($h = 1$ cm) for various rotating angles. c) Relationships between the *x*-, *y*-, and *z*-components of electric displacement and time for various heights at constant lateral and longitudinal positions. The rotating speed of the PMMA sectors was set to be 150 rpm. d) Calculated *x*-, *y*-, and *z*-components of Maxwell's displacement current density for various heights.

in the overlapped region is $+\sigma$. The value of σ was set to be 10 μC m^{-2}. The space distributions of electric displacement field were calculated in the rotation process, and the typical results of electric displacement components in the *x*-, *y*-, and *z*-directions at a constant height for various rotating angles are presented in Figure 1b. The half-cycle results indicate that the electric displacement varies with the rotation of PMMA sectors. The electric displacements at $\theta = 0$ and $\theta = \pi/4$ have the same value though the directions are opposite. Further, the electric displacement fields change periodically with a period of $\pi/2$, which produces a periodic displacement current.

Considering the media polarization, according to Gauss's Law, the electric displacement $\boldsymbol{D}$ can be given by

$$D = \varepsilon_0 E + P \tag{1}$$

where ε_0 is the vacuum permittivity, $\boldsymbol{E}$ is the electric field, and $\boldsymbol{P}$ is the polarization field. The change of $\boldsymbol{D}$ contains two parts: the change of electric field and that of polarization field. The Maxwell's displacement current can be defined as change of electric displacement with respect to time

$$J_D = \frac{\partial D}{\partial t} = \varepsilon_0 \frac{\partial E}{\partial t} + \frac{\partial P}{\partial t} \tag{2}$$

The polarization density $\boldsymbol{P}$ has two contributors: one is from the electric field induced media polarization $\boldsymbol{P}_I = (\varepsilon - \varepsilon_0)\boldsymbol{E}$; and the other is from the polarization due to the presence of surface triboelectric charges $\boldsymbol{P}_S$, which is responsible for the displacement current observed in our experiments. Based on the two equations mentioned above, we can obtain the displacement current density J_D at any point of the space by calculating the $\boldsymbol{D}$–*t* relationship with the finite element (FEM) simulations. The rotation-induced displacement current is the design basis and theoretical reference of such rotary electrodeless TENGs. By decomposing the $\boldsymbol{D}$ and J_D into *x*-, *y*-, and *z*-components, we can obtain the following relations

$$J_D = J_{Dx} + J_{Dy} + J_{Dz} = \frac{\partial D_x}{\partial t} + \frac{\partial D_y}{\partial t} + \frac{\partial D_z}{\partial t} \tag{3}$$

Figure 1c shows the electric displacement components $\boldsymbol{D}_x$, $\boldsymbol{D}_y$, and $\boldsymbol{D}_z$ as functions of time for various heights *h* at constant lateral and longitudinal positions. The rotating speed of the PMMA sectors was set to be 150 rpm. It can be seen that the $\boldsymbol{D}_x$–*t* and $\boldsymbol{D}_z$–*t* curves are periodic waves at any height. When $\boldsymbol{D}_x$ has a positive direction, $\boldsymbol{D}_z$ is negative, and vice versa. However, the $\boldsymbol{D}_y$–*t* curves exhibit a shape of fold lines with a smaller height, but a wavy shape at a larger height. As for height, all of the electric displacement components decrease gradually when the height increases. Through the differentiation of $\boldsymbol{D}_x$, $\boldsymbol{D}_y$, and $\boldsymbol{D}_z$ by *t*, we can obtain the *x*-, *y*-, and *z*-components of Maxwell's displacement current density. The J_{Dx}–*t*, J_{Dy}–*t*, and J_{Dz}–*t* relationships are shown in Figure 1d for various heights. Similar to the $\boldsymbol{D}_y$–*t* curve, the J_{Dx}–*t* and J_{Dz}–*t* curves both have the fold line shape at a smaller height, while the J_{Dy}–*t* curves have a square wave shape. With increasing height, the displacement current components exhibit a wavy shape and also decrease with increasing height.

Besides height, the influences of lateral position x_0 on the electric displacement and displacement current density were also investigated, as shown in **Figure 2**. Figure 2a–c show the relationships between $\boldsymbol{D}_x$, $\boldsymbol{D}_y$, $\boldsymbol{D}_z$, and *t* for various lateral positions x_0 at constant longitudinal position ($y_0 = 0$ cm) and height ($h = 1$ cm). With the increase of x_0, the peak value of $\boldsymbol{D}_x$ first increases and then decreases. The peak values of $\boldsymbol{D}_y$ and $\boldsymbol{D}_z$ also

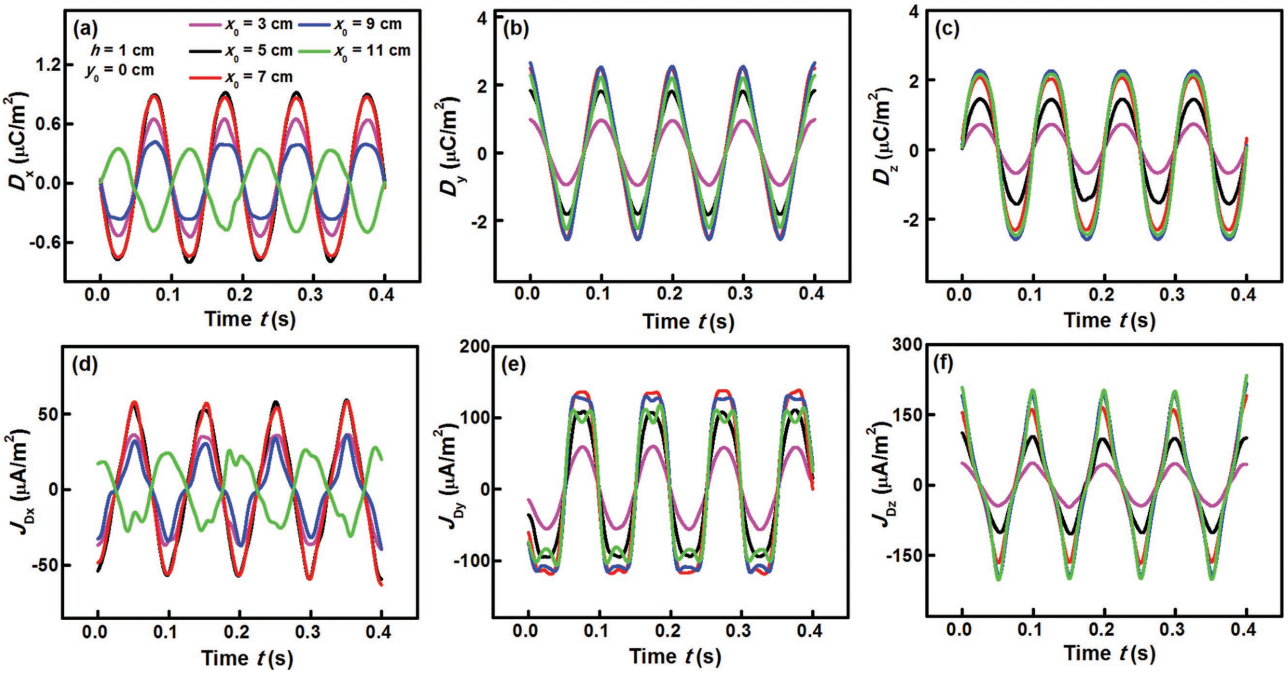

Figure 2. Electric displacement and displacement current for various lateral positions. a–c) Relationships of the *x*-, *y*-, and *z*-components of electric displacement versus time for various lateral positions x_0 at constant longitudinal position ($y_0 = 0$ cm) and height ($h = 1$ cm). Rotating speed of the PMMA sectors was set to be 150 rpm. d–f) Calculated *x*-, *y*-, and *z*-components of Maxwell's displacement current density for various lateral positions x_0.

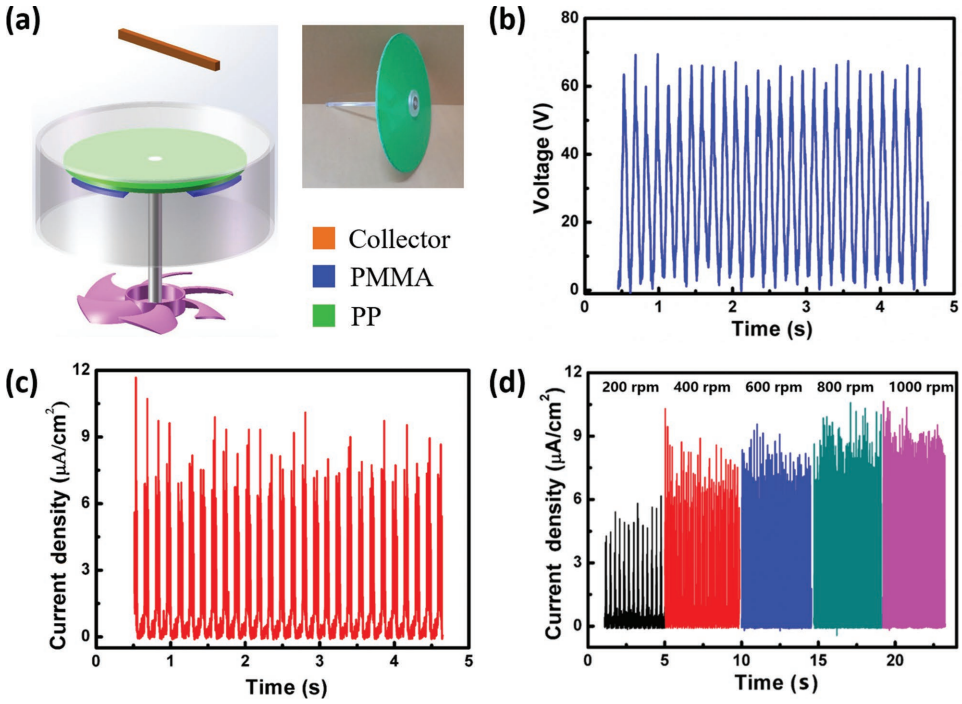

Figure 3. Electrical output characterization of the as-fabricated electrodeless TENG. a) Schematic diagram of the rotary electrodeless TENG with collectors. b) Open-circuit voltage and c) short-circuit current density of the electrodeless TENG. d) Short-circuit current density of the as-designed TENG under different rotating speeds.

first increase, but the subsequent decrease is much slighter. Similar tendencies for the displacement current components J_{Dx}, J_{Dy}, and J_{Dz} can also be observed, as shown in Figure 2d–f. The fold line shapes of D_y, J_{Dz}, and the square wave shape of J_{Dy} appear at a larger x_0. Note that at a large x_0 close to the edge of disk ($x_0 = 11$ cm), the directions of D_x and J_{Dx} become opposite to those at a smaller x_0, which can also be viewed from Figure 1b. Because the surface charge densities are the same for the inner side and outer side of the PMMA sectors, the outer side carries more triboelectric charges. The different charge distributions along the lateral direction cause different electric displacements, including the absolute value and direction. The opposite directions of D_x and J_{Dx} at the disk edge can be attributed to the cooperative action of electric field and polarization field created by surface electrostatic charges at the given height.

Rotation friction between the PP disk and PMMA sectors can produce opposite polarization charges on the tribo-surfaces. During the rotation process, the periodic change of charge distributions causes the space electric displacement field to change periodically, producing the displacement current depending on the space position. In such a rotary electrodeless TENG, the rotation motion induces the redistribution of polarization charges. In fact, as long as the polarization charges can be separated/contacted or redistributed, the displacement current can be produced and transferred even without electrodes and wires. For the simple lateral-sliding mode, the sliding friction between two dielectric materials can induce the time-varying displacement field and displacement current. The detailed results can be found in Figures S1–S3 (Supporting Information).

Here we also demonstrated the wireless output performance of the electrodeless TENG experimentally based on the proposed working mechanism. A rotary electrodeless TENG containing a PP disk, PMMA sectors, and metal collectors was fabricated and schematically shown in **Figure 3**a. The right-hand side presents a photograph of the as-fabricated TENG device. The PP disk acts as a stator and the PMMA sectors with four units adhered to a transparent acrylic axle driven by a governor motor act as the rotator. The diameters of the PP disk and PMMA sectors are respectively 30 and 25 cm, and their thicknesses are both 5 mm. The collectors having several units in a size of 14 mm × 2 mm × 7 mm connected with an edge banding are capable of harvesting electrostatic field energy and converting it into alternating current. Furthermore, the driving force for rotation can be replaced by other forms of mechanical energy in the nature, such as wind, tide, and so on.

Figure 3b,c shows the open-circuit voltage and short-circuit current density of the as-fabricated electrodeless TENG with a rotating speed of 1000 rpm and four groups of collectors, respectively. By integrating rectifiers with collectors, the output current density can reach about 7 μA cm^{-2}, while the voltage remains at a peak value of 65 V, as shown schematically in Figure S4a (Supporting Information). The equivalent circuit diagram including the electrodeless TENG, full-bridge rectifier, and the load is shown in Figure S4b (Supporting Information). The TENG can be represented by the serial connection of an ideal voltage source (V_{OC}) and a capacitor (C). Through the rectifier connected with the collector, the electrical energy can be delivered from the TENG to the load. It should be noted that though only one rectifier is shown here, in the practical operation we could use many rectifiers connected with collectors at different positions to harvest the energy from a larger coverage area. In order to study the influence of rotating

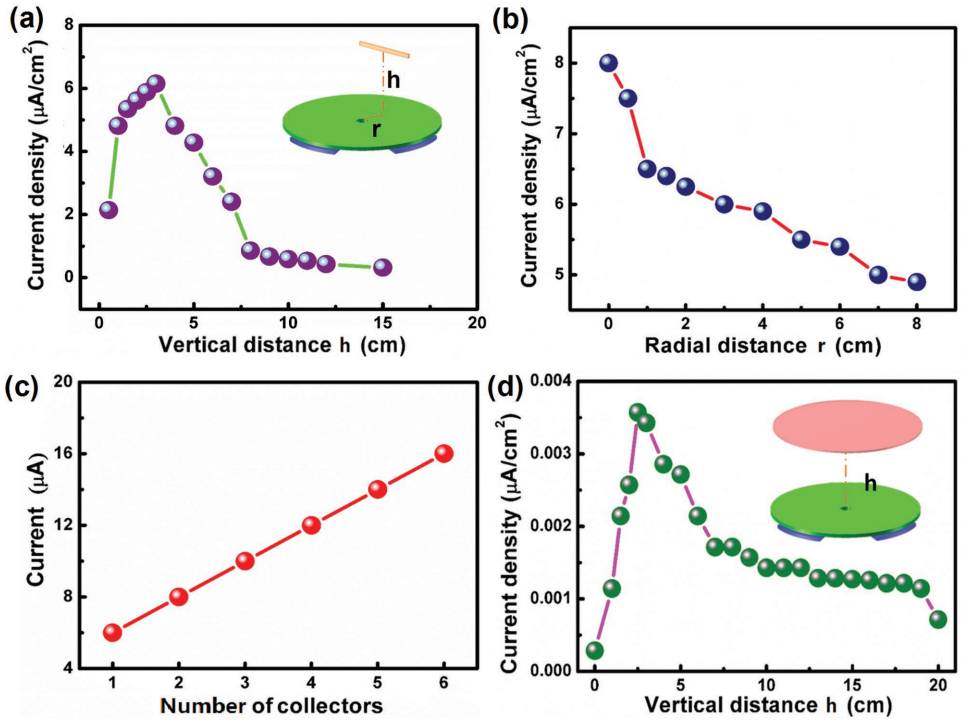

Figure 4. Wireless energy delivery performance for the as-designed electrodeless TENG. a) Dependence of the current density on the vertical distance *h*. b) Dependence of the current density on the radial distance *r*. c) Output current of the TENG with respect to the number of metal collectors. d) Current density of the TENG with a foil-like collector at different vertical distances *h*.

speed on the output performance of the electrodeless TENG, the rotating speed was increased from 200 to 1000 rpm. As shown in Figure 3d, the current density increases proportionally to the rotating speed from 5 to 9 μA cm^{-2}. Besides, a slight change with the rotating speed has also been observed from the output voltage, as demonstrated in Figure S5 (Supporting Information).

Wireless energy delivery performance of the electrodeless TENG was investigated by changing the location or number of collectors. We measured the output current at different collector locations and numbers lasting for 1 min, and then calculated the average value of the current peaks. Output current densities of the collector response at different vertical distances *h* are shown in **Figure 4**a, where the radial distance *r* is 3 cm. The current density initially increases with increasing vertical distance (<3 cm) and then decreases with larger vertical distance. Thus, the vertical distance was kept as 3 cm and the output current density was found to decrease as increasing the radial distance (Figure 4b). Figure 4c demonstrates that the short-circuit current linearly increase with increasing collector number. The output of the wireless power delivery system can be further improved by increasing the collector number or optimizing the structure of the collector.

The strip-shaped collectors can wirelessly collect power owing to the displacement current. The strip-shaped collectors were replaced by a large metal foil-like collector with structural symmetry to compare the wireless energy delivery performance. The aluminum foil with the same size as the PP disk was placed on the top of PP disk at a vertical distance of *h*. Figure 4d shows the current density of the TENG with a foil-like collector at different *h*. Although there is a peak for the current density similar to that from strip-shaped collectors at about $h = 3$ cm, the current density is very low, near to zero. Due to the screening effect of symmetrically distributed Al foil, the electric displacement at the Al foil does not change, and no displacement current is produced. Therefore, to ensure the wireless power deliver performance, the collector should be designed as an asymmetrical structure with respect to the TENG, generating the displacement current by a leakage electric field.

The influence of medium on the wireless power deliver performance was also studied. When the medium is changed, the performance of wireless energy delivery will change. The FEM simulations indicated that when the medium is some lossy materials, the electric displacement and displacement current both decrease compared to a dielectric medium without dielectric loss, implying the decrease of performance for wireless energy delivery. When the medium is further changed to metal materials, the electric displacement and displacement current become very low, and the wireless energy delivery performance is poor.

The wireless power delivery in this work is based on the Maxwell's displacement current generated by an electrodeless TENG. The displacement current resulting from the change of space electric displacement field during the rotation is the underlying mechanism of power generation and delivery. This is different from the traditional capacitive coupling.[21] In a traditional capacitive power transfer system, energy is transmitted by the oscillating electric fields between the transmitter and receiver electrodes, in which the two electrodes form a

capacitor, and an alternating voltage generated by the transmitter is applied to the transmitter electrodes. The alternating potential on the receiver electrode by electrostatic induction causes an alternating current to flow in the load circuit. However, in our wireless power delivery system, there are no two electrodes placed face to face, and there are only metal collectors. The transmitter part consists of two kinds of dielectric materials in relative rotation, and during the rotation the electric displacement field changes in the whole space (not just between two metal plates). There exists the media polarization from the surface triboelectric charges contributing to the displacement current, which is absent in a capacitive coupling. Therefore, the mechanism of wireless power delivery in our system is essentially different.

In addition, the electrodeless TENG designed in our work is different from an electret generator. In the electret generator reported in Boland's paper, the stator is made of an electret film bonded by an aluminum electrode on a quartz wafer, while the rotator has an aluminum electrode on a quartz wafer.[22] There is a gap between the rotator and stator, and the ground lead and power lead of the generator are connected to the ground of stator and test-bed chassis electrically connected to the rotator, respectively. So, in the electret generator, the electrodes and leads both exist, and the current produces across the rotator electrode and ground. However, our TENG has no electrodes and leads, and its device structure with the contacting rotation between stator and rotator is different from the electret generator. There is no wireless energy delivery for the electrets generator, and there is just power generation based on the electrostatic induction. The floating electret layer was designed just to make the surface charges distribute uniformly, not to realize the wireless energy delivery. In our work, we wanted to propose the mechanism of wireless energy delivery based on the Maxwell's displacement current, which is not reported in previous work. Regarding the electrode design, there are no electrodes in our TENG system. One available device structure was designed as an example in this work, and the structure will be next optimized to improve the power delivery.

To demonstrate the capability and feasibility of this wireless energy delivery protocol for practical applications, a rotary electrodeless TENG device was fabricated as pictured in **Figure 5**a. The collectors were constructed from tightly doubled ferroalloy plates which were then fastened to the polytetrafluoroethylene (PTFE) frame and connected to light-emitting diodes (LEDs) to form a lamp. When the lamp was placed above the PP plate in the electric field generated by the electrodeless TENG, the LEDs can be lighted up as shown in the figure. Interestingly, the LEDs can be still lighted up even when the lamp with collectors was moved away from the PP plate until ≈10 cm. The wireless energy delivery can also be demonstrated by powering an electronic watch without a battery, as pictured in Figure 5b. In addition, a flexible electrodeless TENG device can be simply realized by using cloth fabrics as triboelectric materials (Figure 5c), and a wearable electrodeless TENG can be fabricated to harvest the biomechanical energy (Figure 5d and Video S1, Supporting Information). LEDs can be lighted up through the wireless energy delivery based on the Maxwell's displacement current. The flexible electrodeless TENG is not a rotating-mode TENG, but a contact-separation mode TENG. When the cloth fabrics were shaken, two triboelectric materials can contact and separate, causing a change of the space electric displacement field. The cloth fabrics based TENGs have only the structural difference with the rotary TENG, but they both generate the displacement current and realize the wireless energy delivery.

The efficiency of the wireless energy delivery can be defined as the ratio of the harvested energy at the load wirelessly to the output energy from the electrodeless TENG. It is different from the energy conversion efficiency of TENG, which is the ratio of the energy output of the TENG to the energy input for the rotation. The wireless power delivery efficiency depends on a number of factors, such as the distance from the TENG, the size of the collector, and the relative position of the collector. An oversized collector would suppress received current to the load due to the cancellation of internal circular current inside the collector, while a small collector would result in small output power. Since the power delivery relies on the leakage electric field between the segmented structure of the TENG, the collection efficiency is relative low in comparison to the traditional coupled inductors especially at high frequency, but it may be a better choice for low-frequency power delivery (<5 Hz).[23] In this work, the wireless energy transfer can be directed and focused from the TENG to the collector. The rotary electrodeless TENG can induce the change of space electric displacement field, generating the displacement current at the collectors. When we place the collectors at the optimized position, the efficiency can be maximized. The alternating electric displacement field is distributed in the whole space, but the coverage area of our collectors is so limited that we cannot measure the maximum delivery power through the experiments. Although we cannot calculate the maximum efficiency due to many variables, we can get the lowest limit of the maximum efficiency via experiments (Figure S6 and Video S2, Supporting Information). In any case, our goal here is to present a new approach for wireless power delivery.

In summary, we have demonstrated the wireless power delivery via Maxwell's displacement current on the base of an electrodeless TENG. The finite element simulations indicate that the rotation-induced displacement current due to the periodic change of electric displacement fields is the underlying working mechanism of such rotary electrodeless TENG. An electrodeless TENG device containing a PP disk, PMMA sectors, and metal collectors was then experimentally fabricated and tested. The output current density via collectors can reach 7 μA cm^{-2} and the open-circuit voltage reaches 65 V at the vertical distance of 3 cm. The wireless energy delivery behavior was also found to be dependent on the vertical and radial distances. Furthermore, the electrodeless TENG can serve as the power source for driving portable and wearable electronics, opening the applications of the Maxwell's displacement current in modern electronics.

Experimental Section

Fabrication of the Electrodeless TENG: The whole electrodeless TENG device consists of two parts: a rotary TENG and metal collectors. The rotary TENG is mainly composed of a stator (made of PP) and a rotator (made of PMMA) as shown in Figure 3a. The stator was cut with the diameter of 30 cm by the laser cutting technology and immobilized onto

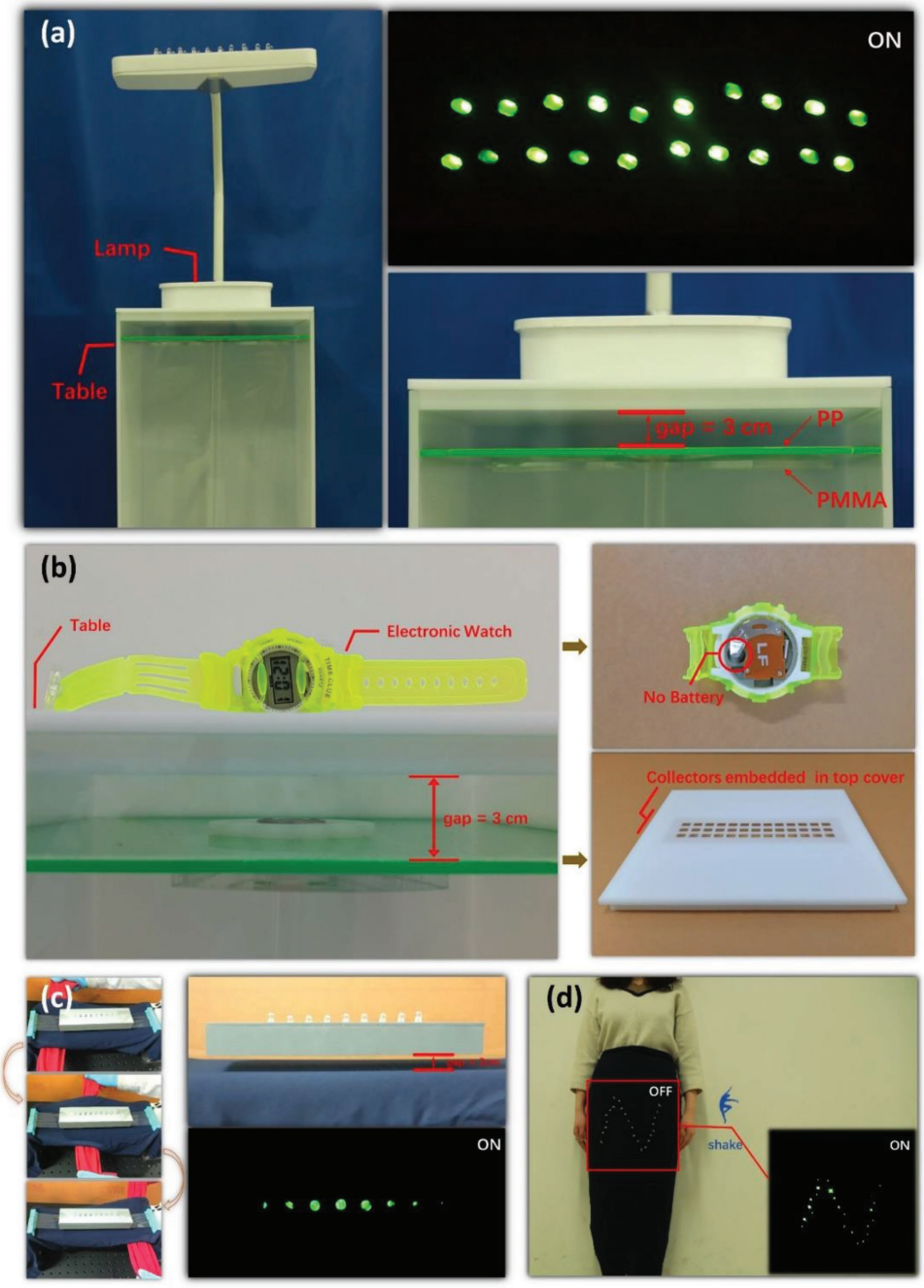

Figure 5. Demonstration of the electrodeless TENG as a wireless power source. a) Photographs of a rotary electrodeless TENG device and a lamp with collectors connected. Optical images of LEDs lighted up. b) An electronic watch powered via wireless energy delivery. c) Photograph of a flexible electrodeless TENG device fabricated by cloth fibers and optical image of LEDs lighted up via wireless energy delivery. d) Photographs of a wearable electrodeless TENG device and lighted LEDs.

the top bearing. The rotator was cut with the diameter of 25 cm and adhered to the same bearing.

Fabrication of the Collector: The collector is an energy collecting device that is made of two pieces of ferroalloy, with the size of 14 mm × 2 mm × 7 mm. Several collectors were connected with an edge banding. When placed in the electrostatic field, the collector is capable of harvesting electrostatic field energy and converting it into alternating current.

Measurement and Characterization: The output voltage and current of the electrodeless TENG were measured by applying an external force with a governor motor (6IK200RGU-CF). A Keithley Model 6514 System Electrometer was used to measure the open-circuit voltage, while an SR570 low-noise current amplifier (Stanford Research System) was used to measure the short-circuit current.

Supporting Information

Supporting Information is available from the Wiley Online Library or from the author.

Acknowledgements

X.C., J.H., and T.J. contributed equally to this work. Research was supported by the "thousands talents" program for pioneer researcher and his innovation team, China, the National Key R & D Project from Minister of Science and Technology (2016YFA0202702, 2016YFA0202704), and National Natural Science Foundation of China (Grant Nos. 51432005, 5151101243, 51561145021). Patents have been filed based on the research results presented in this manuscript.

Conflict of Interest

The authors declare no conflict of interest.

Keywords

displacement current, triboelectric nanogenerators, wearable devices, wireless energy delivery

Received: July 21, 2017
Revised: September 14, 2017
Published online:

[1] K. B. Huang, V. K. N. Lau, *IEEE Trans. Wireless Commun.* **2014**, *13*, 902.
[2] X. Lu, P. Wang, D. Niyato, D. I. Kim, Z. Han, *IEEE Commun. Surv. Tutorials* **2015**, *17*, 757.
[3] C. W. Van Neste, J. E. Hawk, A. Phani, J. A. J. Backs, R. Hull, T. Abraham, S. J. Glassford, A. K. Pickering, T. Thundat, *Wireless Power Transfer* **2014**, *1*, 75.
[4] A. Kurs, A. Karalis, R. Moffatt, J. D. Joannopoulos, P. Fisher, M. Soljačić, *Science* **2007**, *317*, 83.
[5] R. Zhang, C. K. Ho, *IEEE Trans. Wireless Commun.* **2013**, *12*, 1989.
[6] A. Karalis, J. D. Joannopoulos, M. Soljacic, *Ann. Phys.* **2008**, *323*, 34.
[7] S. Ulukus, A. Yener, E. Erkip, O. Simeone, M. Zorzi, P. Grover, K. Huang, *IEEE J. Sel. Areas Commun.* **2015**, *33*, 360.
[8] F. R. Fan, Z. Q. Tian, Z. L. Wang, *Nano Energy* **2012**, *1*, 328.
[9] X. Wen, W. Yang, Q. Jing, Z. L. Wang, *ACS Nano* **2014**, *8*, 7405.
[10] L. Dhakar, P. Pitchappa, F. E. H. Tay, C. Lee, *Nano Energy* **2016**, *19*, 532.
[11] W. Tang, T. Zhou, C. Zhang, F. R. Fan, C. B. Han, Z. L. Wang, *Nanotechnology* **2014**, *25*, 225402.
[12] Z. Quan, C. B. Han, T. Jiang, Z. L. Wang, *Adv. Energy Mater.* **2016**, *6*, 1501799.
[13] L. Xu, Y. Pang, C. Zhang, T. Jiang, X. Chen, J. Luo, W. Tang, X. Cao, Z. L. Wang, *Nano Energy* **2017**, *31*, 351.
[14] S. W. Chen, X. Cao, N. Wang, L. Ma, H. R. Zhu, M. Willander, Y. Jie, Z. L. Wang, *Adv. Energy Mater.* **2016**, *6*, 1501778.
[15] Y. Jie, Q. W. Jiang, Y. Zhang, N. Wang, X. Cao, *Nano Energy* **2016**, *27*, 554.
[16] H. Phan, D.-M. Shin, S. H. Jeon, T. Y. Kang, P. Han, G. H. Kim, H. K. Kim, K. Kim, Y.-H. Hwang, S. W. Hong, *Nano Energy* **2017**, *33*, 476.
[17] D.-M. Shin, E. L. Tsege, S. H. Kang, W. Seung, S.-W. Kim, H. K. Kim, S. W. Hong, Y.-H. Hwang, *Nano Energy* **2015**, *12*, 268.
[18] D.-M. Shin, H. J. Han, W.-G. Kim, E. Kim, C. Kim, S. W. Hong, H. K. Kim, J.-W. Oh, Y.-H. Hwang, *Energy Environ. Sci.* **2015**, *8*, 3198.
[19] Z. L. Wang, *Mater. Today* **2017**, *20*, 74.
[20] Z. L. Wang, T. Jiang, L. Xu, *Nano Energy* **2017**, *39*, 9.
[21] J. Dai, D. C. Ludois, *IEEE Trans. Power Electron.* **2015**, *30*, 6017.
[22] J. Boland, Y.-H. Chao, Y. Suzuki, Y. C. Tai, in *16th IEEE Int. Conf. Micro Electro Mechanical Systems (MEMS)*, Kyoto, Japan **2003**.
[23] Y. L. Zi, H. Guo, Z. Wen, M.-H. Yeh, C. Hu, Z. L. Wang, *ACS Nano* **2016**, *10*, 4797.